Chromatographia (2019) 82:181–196
https://doi.org/10.1007/s10337-018-3662-6

ORIGINAL

Application of Kinetically Optimised Online HILIC × RP-LC Methods Hyphenated to High Resolution MS for the Analysis of Natural Phenolics

Magriet Muller[1] · Andreas G. J. Tredoux[1] · André de Villiers[1]

Received: 17 August 2018 / Revised: 8 November 2018 / Accepted: 15 November 2018 / Published online: 23 November 2018

Abstract

Phenolics are a large group of secondary plant metabolites that are of interest because of their proposed health benefits. The analysis of plant phenolics is challenging due to their extreme structural diversity. Comprehensive two-dimensional liquid chromatography (LC × LC) coupled to high-resolution mass spectrometry (HR-MS) offers a powerful analytical tool for the analysis of such complex mixtures. Especially, the combination of hydrophilic interaction chromatography (HILIC) and reversed-phase liquid chromatography (RP-LC) is attractive for phenolic analysis due to the orthogonal group-type separations attainable. However, online hyphenation of HILIC and RP-LC is complicated by the relative elution strengths of the mobile phases used in both dimensions. Coupled to the inherent complexity of method development in LC × LC, this hampers the more widespread application of HILIC × RP-LC. In this study, a generic HILIC × RP-LC−DAD-MS methodology for phenolic analysis utilising dilution of the first dimension flow and large volume injection in the second dimension is derived by kinetic optimisation of experimental parameters to provide maximum performance. The scope of the experimental configuration is demonstrated by its application to the analysis of rooibos tea, wine and grape samples containing a range of different flavonoid and non-flavonoid phenolic classes. Using this approach, excellent chromatographic performance was obtained, and a total of 149 phenolic compounds were tentatively identified in the investigated samples based on retention data in two dimensions, UV–Vis spectral as well as high- and low collision energy HR-MS data (72 in grape seeds, 32 in rooibos tea and 45 in wine and grapes) with minimal method development time. The results confirm the applicability of the proposed methodology for the detailed screening of phenolic constituents in natural products.

Published in Chromatographia's 50th Anniversary Commemorative Issue.

Electronic supplementary material The online version of this article (https://doi.org/10.1007/s10337-018-3662-6) contains supplementary material, which is available to authorized users.

✉ André de Villiers
ajdevill@sun.ac.za

[1] Department of Chemistry and Polymer Science, Stellenbosch University, Private Bag X1, Matieland 7602, South Africa

Graphical Abstract

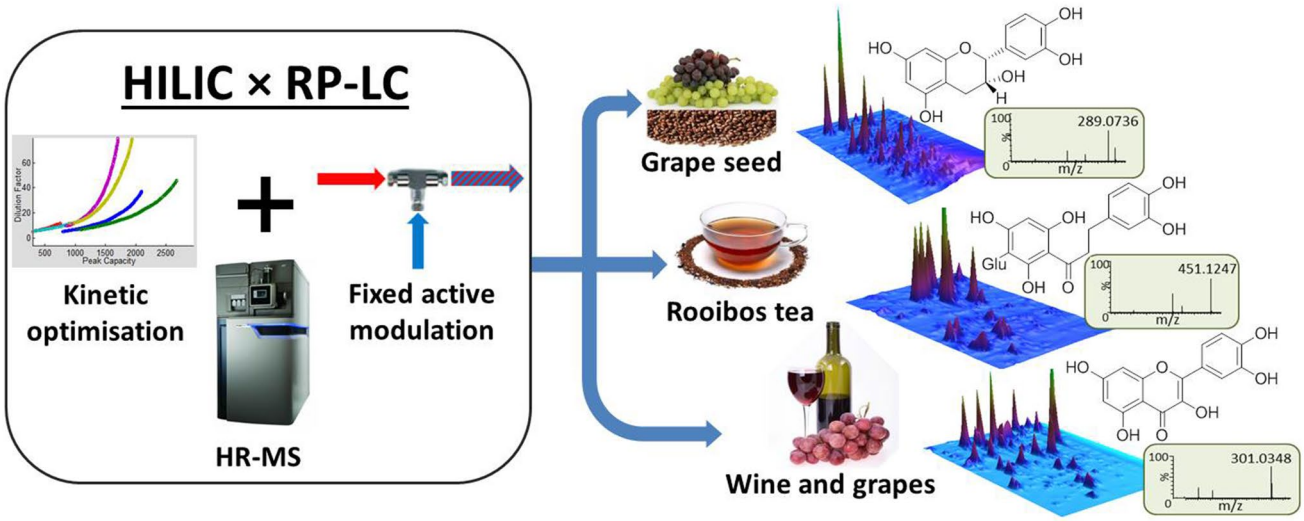

Keywords Comprehensive two-dimensional liquid chromatography (LC × LC) · Hydrophilic interaction chromatography (HILIC) · Reversed phase liquid chromatography (RP-LC) · High resolution mass spectrometry (HR-MS) · Online · Phenolics · Flavonoids

Introduction

The study of the phenolic composition of natural products is of interest in light of the bioactive roles that these compounds play in plants and as part of the human diet [1]. Due to the complexity of plant phenolics, however, conventional high performance liquid chromatography (HPLC) often does not provide sufficient separation for these samples. Comprehensive two-dimensional liquid chromatography (LC × LC) has for this reason found increasing application in the study of plant phenolics in recent years [2–4]. While the availability of commercial instrumentation has greatly improved the implementation of LC × LC in many laboratories, the complexity of LC × LC method development continues to limit the more widespread use of the technique. This is because method development in LC × LC requires consideration of a large number of intricately related experimental parameters and instrumental restraints and their effects on achieving mutually incompatible goals in terms of peak capacity, analysis time and dilution.

To avoid the pitfalls associated with trail-and-error LC × LC method development, which is often counter-intuitive because of the complex relationship between experimental parameters, several step-wise LC × LC method optimisation schemes have been reported [5–11]. A comprehensive kinetic optimisation protocol for online LC × LC was reported by Vivó-Truyols et al. [8], who used multi-parameter Pareto-optimisation to derive optimal LC × LC experimental conditions. A similar approach has subsequently been used to derive optimal conditions for the RP-LC × RP-LC separation of peptides [10, 11]. Recently, Pirok et al. [12] reported a method that also allows for the optimisation of mobile phase gradients to maximise resolution and orthogonality.

In the context of phenolic analysis, the combination of hydrophilic interaction chromatography (HILIC) and reversed-phase LC (RP-LC) has been shown to be especially beneficial due to the high degree of orthogonality associated with this combination for many classes of phenolics [13, 14]. Method development for online HILIC × RP-LC is, however, particularly challenging due to the devastating effect injection of organic-rich HILIC mobile phase can have on the performance of the second dimension (^{2}D) RP-LC separation. In cases where the mismatch between first dimension (^{1}D) mobile phase (effectively the sample solvent for transferred fractions) and ^{2}D separation is less severe (such as RP-LC × RP-LC systems for example), well known equations to model injection band broadening have been used with some success in method optimisation protocols [5, 8, 10, 11]. However, we have recently shown that under extreme sample solvent mismatch conditions such as encountered in HILIC × RP-LC, predictions using these equations, both for direct transfer of undiluted fractions and large volume injections of diluted fractions, are inaccurate [15]. In such cases, more sophisticated methods, such as reported

by Stoll et al. [16], may be required to accurately model the effect of injection band broadening. Unfortunately, incorporation of such approaches into method development protocols is currently not feasible due to impractical computational power requirements.

A number of strategies have been devised to circumvent problems arising from mobile phase mismatches in LC × LC. These so-called 'active modulation' approaches include basic solutions such as splitting the ^{1}D effluent [9, 17] and diluting the ^{1}D effluent with a weak ^{2}D mobile phase [18], as well as more technically advanced options such as the use of trapping columns [19, 20], thermally assisted modulation [21], membrane evaporation [22] or vacuum evaporation [23]. While the latter four methods can greatly improve the performance of LC × LC separations, they are difficult to implement and require dedicated method development protocols. On the other hand, simpler active modulation strategies such as splitting and/or dilution of the ^{1}D effluent can effortlessly be incorporated into method optimisation schemes [9–11, 15].

Since accurate prediction of injection band broadening in HILIC × RP-LC is not feasible using current theoretical models, an alternative approach is to first establish experimental conditions where injection band broadening is effectively avoided. Provided that these conditions are met, injection effects can then be disregarded during method optimisation. We recently reported a Pareto-based kinetic optimisation program for HILIC × RP-LC separations [15] which incorporates dilution of the ^{1}D effluent to negate the effect of injection band broadening in the ^{2}D under previously established conditions. The program uses the theoretical relationships between various chromatographic parameters and analyte properties to predict performance for any set of conditions and, by comparing the performance of numerous theoretical combinations, is able to derive optimal experimental conditions for any given separation in terms of analysis time, peak capacity and dilution. This program was use to compare the performance of different column dimensions and to derive optimal conditions for the online HILIC × RP-LC separation of procyanidins. In the current contribution, we demonstrate the application of this kinetic optimisation protocol in combination with fixed active modulation requirements to derive a generic HILIC × RP-LC methodology for the analysis of complex natural phenolic mixtures. Hyphenation of optimised HILIC × RP-LC methods to UV and high resolution mass spectrometric (HR-MS) detection is shown to provide a powerful analytical methodology for the detailed analysis of a wide range of phenolic compounds, including monomeric and oligomeric flavonoids, phenolic acids and chalcones in several natural product extracts.

Experimental

Reagents and Materials

HPLC grade methanol (MeOH), formic acid and diethyl ether were purchased from Sigma-Aldrich (Steinheim, Germany) and HPLC grade acetonitrile (ACN) from ROMIL (Waterbeach Cambridge, England). Deionised water was obtained using a Milli-Q water purification system (Millipore, Milford, MA, USA). Grape seed extracts were provided by the Institute of Wine Biotechnology (IWBT, Stellenbosch University), dry rooibos tea samples by the Central Analytical Facility (CAF, Stellenbosch University) and experimental grape and wine samples (both Shiraz, 2016 vintage) were supplied by the Department of Viticulture and Oenology (Stellenbosch University).

Sample Preparation

Grape Seeds

Grape seeds were separated from the berries and washed with water. The seeds were crushed using a homogenizer and extracted with a 2:1 (v/v) acetone/water solution in a ratio of 1:10 (sample:extraction solvent) for 24 h at 4 °C [24]. After freeze-drying, the sample was reconstituted in MeOH (1000 ppm), filtered through a 0.45-µm hydrophilic PVDF filter membrane (Millipore) and diluted to 75% ACN.

Rooibos Tea

Dried tea leaves [2 g each of three unfermented and one fermented sample(s)] were soaked overnight in a 50% MeOH solution containing 1% formic acid (15 mL) [25]. The mixtures were sonicated for 1 h and centrifuged for 5 min. Each sample was diluted to 80% ACN prior to injection.

Wine

100 mL of the wine sample was extracted with 3 × 100 mL diethyl ether and evaporated under vacuum at room temperature until less than 1 mL remained [26]. The remaining liquid was reconstituted to 1 mL with MeOH and diluted to 80% ACN.

Grapes

Frozen whole grapes (50 g) were pitted and crushed using a mortar and pestle. The crushed pulp and skins were sonicated for 2 h in 100 mL 0.1% formic acid methanol/water (30/70, v/v) and centrifuged for 5 min. The supernatant

was extracted with 3 × 100 mL diethyl ether and evaporated under vacuum at room temperature to less than 0.5 mL. The remaining liquid was reconstituted to 0.5 mL with MeOH and diluted to 80% ACN.

Instrumentation

A schematic illustration of the instrumental configuration used is presented in Fig. S1 (Supporting Information, SI). HILIC × RP-LC analyses were performed using a Waters CapLC 920 pump and autosampler (equipped with a 2-µL loop) in the ^{1}D (Waters, Milford, MA, USA), an Agilent 1290 Infinity II binary pump in the ^{2}D and a 2-position/8-port valve equipped with two 80-µL loops as interface between the two dimensions (Agilent Technologies, Waldbronn, Germany). An Agilent 1100 isocratic pump was used to dilute the ^{1}D eluent before the valve and the ^{2}D column was placed in an Agilent 1200 column oven. UV–Vis spectra were recorded between 190 and 640 nm (80 Hz) using an Agilent 1290 Infinity II DAD detector (1 µL flow cell). The system was coupled to a Waters Synapt G2 quadrupole time-of-flight (Q-TOF) mass spectrometer operated in negative ionisation mode. The following ionisation parameters were used: capillary voltage: 2.5 kV; cone voltage: 15 V; source temperature: 120 °C; cone gas flow (N_2): 50 L h^{-1}; desolvation gas flow (N_2): 650 L h^{-1}; desolvation temperature: 275 °C. The system was operated in MS^{E} mode, which allows the acquisition of both low (4 eV) and high (ramped from 10 to 30 eV) collision energy data alternately in a single analysis. Data were recorded in the range of 150–2000 amu using a scan time of 0.2 s. Ion mobility (IM) separations were achieved using nitrogen as drift gas at a flow of 90 mL min^{-1} (3.27 mbar), with a He flow of 180 mL min^{-1} (1410 mbar) in the He cell. The mobility T-Wave velocity and wave height were 448 m s^{-1} and 37.1 V, respectively, and the transfer velocity was 380 m/s. For further details on the IM separation, the reader is referred to [27].

Leucine enkephalin (m/z = 554.2615) was used as the lock mass for accurate mass determination. The CapLC was controlled by MassLynx software (v4.0, Waters); the Q-TOF was controlled by MassLynx software (v4.1, Waters) and the rest of the modules (including the valve) by OpenLab CDS software (Agilent). Contour plots were constructed using LC Image (v2.6, GC Image LLC, Nebraska, USA).

Chromatographic Conditions

All ^{1}D separations were performed on a Xbridge Amide column (150 × 1.0 mm, 1.7 µm, Waters) using mobile phases consisting of (A) 0.1% formic acid in ACN and (B) 0.1% formic acid in water at a flow rate of 11 µL min^{-1}. Different ^{1}D gradients were used for each sample, as outlined in Table 1. The ^{1}D eluent was diluted with 0.1% formic acid in water at a flow rate of 99 µL min^{-1} (10 × dilution) prior to entering the modulation valve.

In the ^{2}D, a Kinetex C_{18} column (50 × 3.0 mm, 1.7 µm, Phenomenex, Torrance, USA) was used for the analysis of the grape seed sample, and a Zorbax Eclipse Plus C_{18} column (50 × 3.0 mm, 1.8 µm, Agilent) was used for analysis of the tea, wine and grape samples. In ^{2}D, the mobile phases consisted of (A) 0.1% formic acid in water and (B) ACN. All ^{2}D columns were thermostatted at 50 °C. A modulation period of 0.56 min was used for all analyses with the ^{2}D flow rate and gradients as indicated in Table 1. For the grape seed sample, the ^{2}D column effluent was split 1:5 after the UV detector, resulting in a flow of 0.5 mL min^{-1} to the MS. For all other samples, the effluent was split 1:4 between the MS and UV detectors.

Calculations

All computations were performed using in-house written Matlab R2010a (The Mathworks, Natick, USA) scripts, with the results exported to Excel. For a detailed description of the equations used to derive the optimum chromatographic conditions in terms of peak capacity, analysis time and total dilution factor, the reader is referred to our previous study [15]. A list of all the values used in the optimisation procedure is provided in Table S1.

Table 1 Gradient conditions used for the HILIC × RP-LC separations of each of the investigated samples

Sample	^{1}D flow rate	^{1}D gradient	^{2}D flow rate	^{2}D gradient
Grape seed	11 µL min^{-1}	2–10% B in 0–5 min; 10–35% B in 5–45 min; 35–90% B in 45–60 min; 90% B from 60 to 70 min	3 mL min^{-1}	1–45% B in 0–0.38 min; 45–100% B in 0.38–0.39 min; 1% B from 0.39 to 0.56 min
Rooibos tea	11 µL min^{-1}	2–10% B in 0–4 min; 10–40% B in 4–45 min; 40–90% B in 45–60 min; 90% B from 60 to 70 min	2.6 mL min^{-1}	1–45% B in 0–0.35 min; 45–100% B in 0.35–0.36 min; 1% B from 0.36 to 0.56 min
Wine and grapes	11 µL min^{-1}	2–27% B in 0–45 min; 27% B from 45 to 50 min	2.6 mL min^{-1}	1–45% B in 0–0.35 min; 45–100% B in 0.35–0.36 min; 1% B from 0.36 to 0.56 min

Results and Discussion

Derivation of Optimal HILIC × RP-LC Separation Conditions

Chromatographic conditions for the HILIC × RP-LC separations were derived using a predictive kinetic optimisation program previously described [15]. As with most kinetic optimisation protocols, this methodology requires prior selection of stationary and mobile phases in both dimensions to optimise selectivity prior to kinetic optimisation. Alternative approaches have been reported to optimise mobile phase gradients and therefore selectivity in LC × LC [12]; in the present work, these were briefly optimised in 1D mode prior to kinetic optimisation of their combination in LC × LC. In addition, the protocol requires information regarding the retention behaviour (LSS parameters) and kinetic performance (plate height parameters) of the target analytes under the investigated conditions. For the purposes of this work, analyte constants for phenolic compounds were obtained from previous studies, as described below.

In [15], it was shown that the extent of injection band broadening in the ^{2}D was negligible for weakly retained flavanols ($^2k_w = 11.8$ and 32.9, where k_w is the retention factor in pure weak solvent) as long as the ^{1}D HILIC mobile phase was diluted 10 times with water and the injection (fraction) volume was limited to less than 30% of the ^{2}D column void volume ($^2V_0$). Since similar retention behaviour was expected for most other classes of phenolics in the studied samples, the same fixed active modulation requirements were used in the derivation of the proposed generic methodology (Table S1). The validity of this assumption is confirmed by the experimental results reported below. It should be noted that active modulation requirements such as the dilution factor depend strongly on the retention behaviour of compounds in the ^{2}D, and that these should therefore ideally be determined for the target analytes under investigation. While the current findings can be considered generally applicable to phenolics, they are not generic for all compound classes.

For accurate performance prediction using the Pareto-optimisation method, information relating to the target analytes (i.e., plate height terms, diffusion coefficients (D_m's) and linear solvent strength (LSS) parameters) is required. However, to experimentally determine these parameters for all target analyte classes in the investigated samples on different stationary phases would be impractical, as is indeed the case in many LC × LC studies. It was, however, shown [15] that although the accuracy of the predicted performance depends on the analyte constants used as input, the optimal chromatographic conditions do not differ greatly as a function of these values. This means that approximated analyte constants can be used as input to derive kinetically optimal conditions. Therefore, since the goal of kinetic optimisation in the current study was to derive optimal experimental conditions—as opposed to predicting the attainable performance—analyte constants for a series of oligomeric procyanidins [degree of polymerisation (DP) 1–5] previously determined on diol HILIC and superficially porous [15] and fully porous [28] C_{18} RP-LC columns were used for method optimisation in the present work (Table S1). These compounds, as the main constituents of grape seed tannins, are ideal reference compounds for this particular sample. However, they are also suitable model compounds for phenolics in general since they share chemical properties with flavonoids and include high molar mass compounds (up to 1442) to accommodate the chromatographic behaviour of oligomeric and highly glycosylated species of similar masses. Furthermore, because the required gradient span ($\Delta\varphi$) depends on the retention behaviour (LSS parameters) of the target analytes, the gradients required on the columns used to determine the employed LLS parameters were utilised in the optimisation. The total analysis time used for kinetic method optimisation was set to 70 min, which is near the maximum time the MS could record drift time filtered MS data.

For method optimisation, two 1-mm internal diameter (i.d.) ^{1}D columns and four ^{2}D columns of different dimensions and packed with superficially or fully porous particles were selected. These columns were selected primarily based on their availability and the suitability of their dimensions for high resolution HILIC × RP-LC separations [15]. For a detailed description of the columns considered during optimisation, refer to Section S1 in the SI. The resultant Pareto fronts presented in Fig. S2 show the optimal performance attainable for different combinations of the studied columns in terms of practical peak capacity (corrected for ^{1}D undersampling) as a function of total dilution for a 70-min analysis time. Based on the Pareto fronts for these columns (Fig. S2) calculated using the parameters listed in Table S1, we selected the 150 × 1.0 mm, 1.7 µm column in the ^{1}D, since this column provided better performance than the 250 × 1.0 mm, 5 µm column for all column combinations due to the smaller particle size. An amide column of the former dimensions was used for all 2D analyses, since this phase has been shown to offer good performance for anthocyanins [29] and procyanidins [30]. In the ^{2}D, two different columns were selected: a Kinetex C_{18} (50 × 3.0 mm) column packed with 1.7 µm superficially porous particles was used for the grape seed analysis, and a Zorbax Eclipse Plus C_{18} (50 × 3.0 mm) column packed with 1.8 µm fully porous particles for the analysis of the tea, wine and grape samples. Although the combination of the 1.7 µm superficially

porous column with the 1 mm 1.7 µm ^{1}D column provides the best predicted performance (Fig. S2, green line), the lifetime of the former column was found to be limited under LC × LC conditions (~ 30 h). The superficially porous column was therefore only used for the analysis of the most complex sample investigated here, the grape seed sample. In contrast, a column of the same dimensions but packed with 1.8 µm fully porous particles, although less performant than the superficially porous phase, was found to be more stable and was therefore used for the separation of the less complex grape, wine and tea samples. The experimental conditions selected for analysis of the samples ("Chromatographic conditions" section) correspond to the two marked points (labelled #1 for the grape seed sample and #2 for tea, wine and grape samples) lying on the relevant Pareto fronts for the 150 × 1.0 mm, 1.7 µm × 50 × 3.0 mm, 1.7 µm and 150 × 1.0 mm, 1.7 µm × 50 × 3.0 mm, 1.8 µm column combinations (Fig. S2). These conditions were selected based on maximum separation performance (practical peak capacities of ~ 2000 to 2600) attainable for an acceptable total dilution factor of ~ 6×. The optimal experimental conditions selected for both column combinations are surprisingly similar (Table 1, Fig. S2), with identical ^{1}D conditions and modulation times, although the ^{2}D flow rate was slightly higher on the 1.7 µm superficially porous phase. The conditions selected for the configuration incorporating the 1.8 µm fully porous ^{2}D column involved a lower ^{2}D flow rate to provide the same total dilution, which means that the effective ^{2}D gradient time was therefore slightly shorter on this column. The longer ^{2}D gradient time, coupled with the good plate height behaviour of the 1.7 µm superficially porous column, is responsible for the higher predicted peak capacity compared to the configuration with the 1.8 µm fully porous column of the same dimensions (2670 vs. 2040).

Following selection of experimental conditions based on kinetic considerations, ^{1}D gradient profiles for each sample were tuned based on the peak distribution(s) obtained from one or two scouting experiments employing linear gradients of differing initial and final mobile phase compositions at the optimised ^{1}D flow rate of 11 µL min^{-1}. A generic ^{2}D gradient (1–45% ACN) was used for all samples. Although further optimisation of the respective gradients for each sample may improve the 2D separations reported here, this would come at the expense of increased method development time and was therefore not explored.

Results obtained for the analysis of each of the studied samples using these kinetically optimised conditions are discussed in the following sections. Examples of the UV and MS contour plots obtained for each of these samples are presented in Fig. S3 (SI). Comparison of these contour plots shows a noticeable loss in resolution for the MS data, which is due to both unavoidable post-column band broadening in the MS flowpath and the relatively slow acquisition rate (5 Hz) of the MS compared to UV detection (80 Hz). Although the TOF-MS instrument is capable of faster acquisition rates, for the mass range used here higher scan speeds result in a significant decrease in signal-to-noise ratios and were therefore not used. Nevertheless, using the drift time filtered MS data, we were able to obtain clean low and high collision energy MS data for partially co-eluting compounds, which simplified compound identification; this aspect is addressed in more detail in another contribution [27]. Examples of the UV and MS spectra used to tentatively identify selected compounds in each of the samples are given in Fig. S4 (SI).

Grape Seed

Grape seeds are a rich source of oligomeric procyanidins. The analysis of these compounds is particularly challenging due to the large number of isomeric species involved [31–33]. While grape seed procyanidins are comprised of only four isomeric flavanol building blocks—catechin and epicatechin and their respective galloylated derivatives—variation in the type of interflavan linkage (C_4–C_6 or C_4–C_8), the order of connecting units as well as the degrees of polymerisation and of galloylation leads to the extreme structural diversity of grape seed condensed tannins (Fig. 1) [31]. Indeed, although grape seed procyanidins have been the subject of several LC × LC studies [32, 34, 35], their complete characterisation remains an elusive goal.

The UV contour plot (280 nm) obtained for the HILIC × RP-LC separation of grape seed procyanidins is shown in Fig. 2. The necessity for higher resolving power than provided by 1D LC is evident from the complexity of the contour plot. In the HILIC dimension procyanidins are separated according to DP (as indicated by the circles in Fig. 2), while RP-LC provides isomeric separation the ^{2}D.

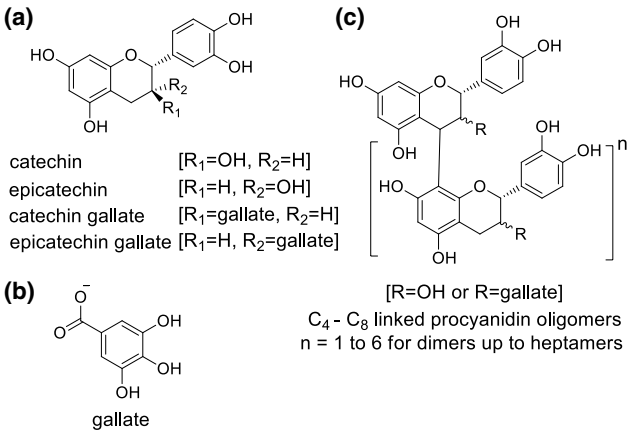

Fig. 1 Chemical structures of the procyanidins detected in grape seeds

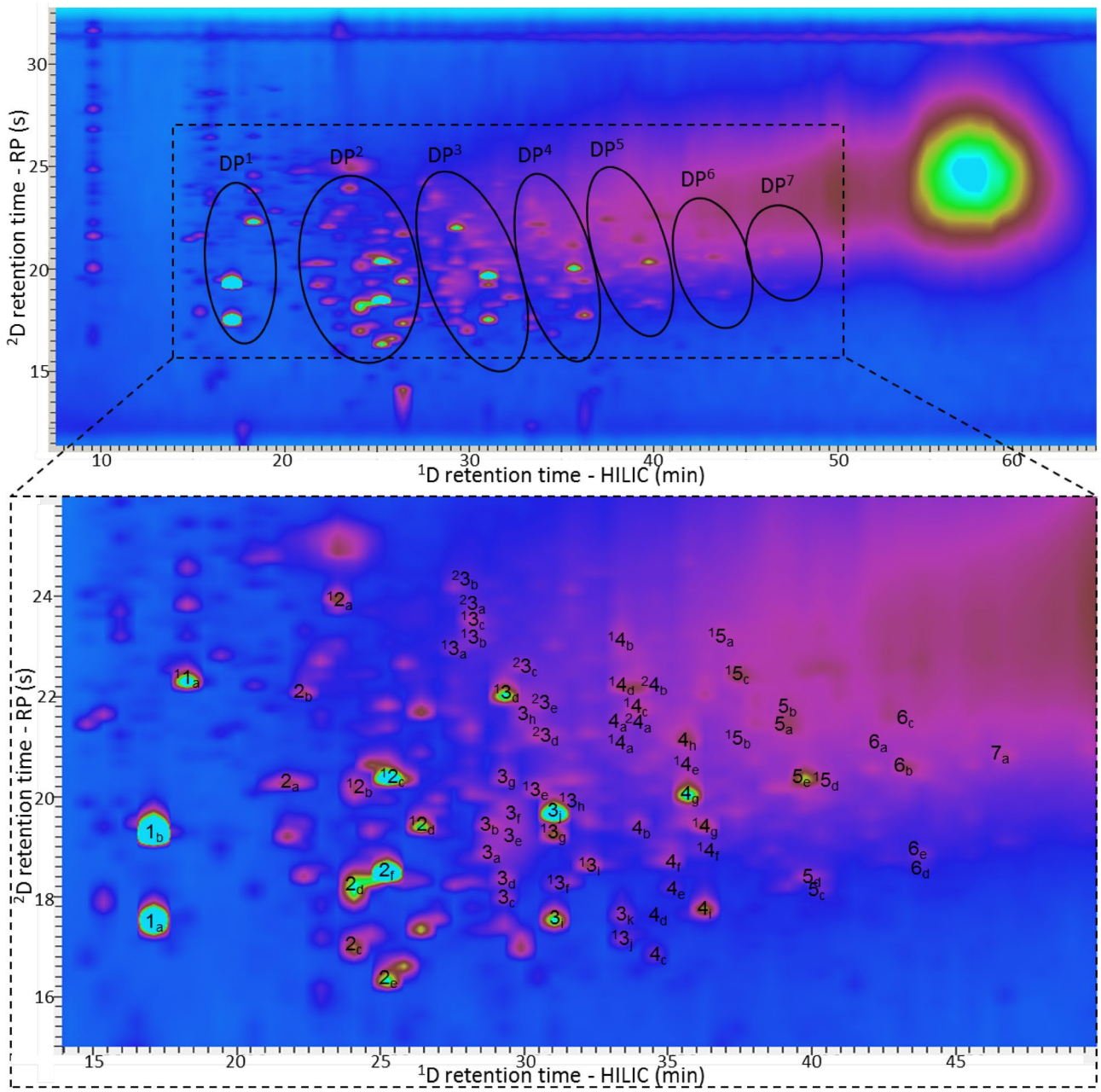

Fig. 2 UV contour plot (280 nm) for the HILIC × RP-LC separation of grape seed procyanidins. The top figure shows the full contour plot with the marked section enlarged below. Circles indicate retention windows for procyanidins of the specified degrees of polymerisation (DP^x). In the notation ${}^{Y}X_{Z,}$ X indicates the degree of polymerisation, Y the degree of galloylation (omitted if $Y=0$) and Z distinguishes isomers. Labelled peaks correspond to Table 2 with the retention times provided in Table S2 (SI). Reprinted (adapted) with permission from [27]. Copyright 2018 American Chemical Society

This structured elution pattern is one of the advantages of HILIC × RP-LC separation for procyanidins [32]. However, it is also clear that separation in both dimensions becomes progressively worse with increasing DP due to the exponential increase in the number of possible isomeric structures. This is evident from the unresolved polymeric 'hump' observed in the high MW region at the end of the HILIC separation.

UV data can be used to distinguish procyanidins from other compounds present in the grape seed sample. However, since the UV–Vis spectra for all procyanidins are similar, they cannot be used to differentiate between procyanidin species. Mass spectrometry data are therefore indispensable for the identification of individual procyanidin molecular species. Hyphenation of HILIC × RP-LC separation to HR-MS detection was therefore used to tentatively identify

Table 2 Summary of procyanidin species detected in a grape seed extract

Label[a]	Compound(s)[b]	DP	DG	Molecular formula $[M-H]^-$	$[M-H]^-$	$[M-2H]^{2-}/2$	Error (ppm)[c]
$\mathbf{1}_{a}$	Catechin	1	0	$C_{15}H_{13}O_{16}$	289.0712		0.7
$\mathbf{1}_{b}$	Epicatechin	1	0	$C_{15}H_{13}O_{16}$	289.0712		2.1
$^{1}\mathbf{1}_{a}$	Epicatechin-gallate	1	1	$C_{22}H_{17}O_{10}$	441.0822		-0.9
$\mathbf{2}_{a–f}$	Procyanidin dimers	2	0	$C_{30}H_{25}O_{12}$	577.1346		0.9
$^{1}\mathbf{2}_{a–d}$	Procyanidin dimer monogallates	2	1	$C_{37}H_{29}O_{16}$	729.1456		1.8
$\mathbf{3}_{a–k}$	Procyanidin trimers	3	0	$C_{45}H_{37}O_{18}$	865.1980		1.2
$^{1}\mathbf{3}_{a–j}$	Procyanidin trimer monogallates	3	1	$C_{52}H_{41}O_{22}$	1017.2089		-1.4
$^{2}\mathbf{3}_{a–e}$	Procyanidin trimer digallates	3	2	$C_{59}H_{46}O_{26}$	1169.2195	584.1060	1.2
$\mathbf{4}_{a–i}$	Procyanidin tetramers	4	0	$C_{60}H_{49}O_{24}$	1153.2614		3.5
$^{1}\mathbf{4}_{a–g}$	Procyanidin tetramer monogallates	4	1	$C_{67}H_{54}O_{28}$	1305.2622	652.1323	-0.8
$^{2}\mathbf{4}_{a–b}$	Procyanidin tetramer digallates	4	2	$C_{74}H_{58}O_{32}$	1457.2726	728.1378	1.4
$\mathbf{5}_{a–e}$	Procyanidin pentamers	5	0	$C_{75}H_{62}O_{30}$	1441.3137	720.1584	0.3
$^{1}\mathbf{5}_{a–d}$	Procyanidin pentamer monogallates	5	1	$C_{82}H_{66}O_{34}$	1593.3317	796.1639	0.5
$\mathbf{6}_{a–e}$	Procyanidin hexamers	6	0	$C_{90}H_{74}O_{36}$		864.1920	1.2
$\mathbf{7}_{a}$	Procyanidin heptamer	7	0	$C_{105}H_{86}O_{42}$		1008.2219	0.5

Compound labels correspond to Fig. 2 and Table S2 in the SI, where the retention data for individual compounds of each class detected are listed

DP degree of polymerisation, *DG* degree of galloylation

[a]Superscripts indicate degree of galloylation, numbers indicate degree of polymerisation and subscripts differentiate between isomers

[b]Sequence of monomeric units in isomeric compounds unknown

[c]Mass error (in parts per million) of the main isomer for each species

72 procyanidin species present in the grape seed extract based on accurate mass data (Table 2). These include procyanidins of a DP up to 7, with varying degrees of galloylation. The HILIC and RP-LC retention times of individual compounds identified in this manner are listed in Table S2 (SI). While the presence of higher DP compounds could be established based on MS data, these were not resolved as individual peaks [32].

Rooibos Tea

Rooibos tea products have attracted growing attention due to their acclaimed health-promoting benefits [36]. This herbal tea originates from the indigenous South African rooibos plant, *Aspalathus linearis*, and is produced from either the fermented (oxidised) or unfermented (green) plant material [37]. Rooibos tea contains a diverse range of phenolic compounds, including flavones, flavanones, flavonols and dihydrochalcones, with some compounds being unique to rooibos (Fig. 3). This phenolic complexity has led to several 1D LC, LC×LC and even capillary zone electrophoresis (CZE) methods being reported for the analysis of rooibos tea phenolics [25, 36, 38–42]. In addition to the species used for commercial rooibos production, several subforms or ecotypes adapted to different geographical locations have been identified [25]. In this study, two of these ecotypes originating from the Wupperthal district in the Western Cape province of South Africa [25] were analysed, along with commercial fermented and unfermented samples.

The HILIC×RP-LC-UV contour plots at 280 nm for the four rooibos tea samples are presented in Fig. 4. Excellent separation of rooibos phenolics is again evident from this figure, with highly glycosylated species generally grouped by their high retention in the HILIC dimension. For these samples, some evidence of an inverse relationship between HILIC and RP-LC retention is evident from the contour plots. The separation could therefore be further improved using reverse shifted gradients [43], where the % organic modifier in RP-LC is systematically decreased during the ^{1}D gradient, although this was not attempted in the present work since the goal was to illustrate how the kinetically optimised HILIC×RP-LC methods are applicable to the analysis of a wide range of phenolic mixtures. Tentative identification of the separated compounds was based on comparison of retention times, UV spectra, accurate mass MS data and MS^{E} fragmentation patterns with literature reports [25, 38, 39] (Table 3).

The contour plot of the fermented commercial tea sample (Fig. 4b) is noticeably different from the unfermented sample (Fig. 4a), with the former containing overall lower levels of phenolics (based on peak area). During fermentation, aspalathin (**20**) is converted to orientin (**18**) and isoorientin (**19**) via the intermediate flavanones eriodictyol-8-*C*-glucoside (**11**) and eriodictyol-6-*C*-glucoside (**12** and **13**) [44]. While

Fig. 3 Structures of some of the phenolic compounds identified in rooibos. Numbers correspond to the labels in Fig. 4. *C-glc C*-linked glucoside, *O-glc O*-linked glucoside

Dihydrochalcones

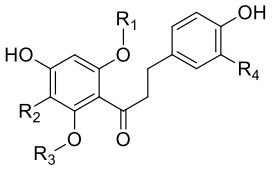

20) Aspalathin [R_1=R_3=H, R_2=*C*-glc, R_4=OH]
24) Nothofagin [R_1=R_4=H, R_2=*C*-glc, R_3=H]
31) Phloridzin [R_1=R_2=R_4=H, R_3=*O*-glc]
32) Sieboldin positional isomer [R_1 or R_3=*O*-glc, R_2=H, R_4=OH]

Flavanones

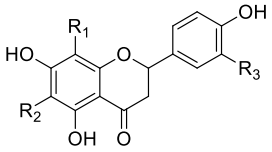

11) (R)-Eriodictyol-8-*C*-glucoside [R_1=*C*-glc, R_2=H, R_3=OH]
12) (S)-Eriodictyol-6-*C*-glucoside [R_1=H, R_2=*C*-glc, R_3=OH]
13) (R)-Eriodictyol-6-*C*-glucoside [R_1=H, R_2=*C*-glc, R_3=OH]

Flavonols

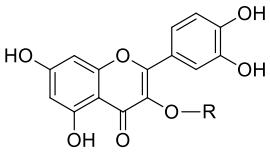

7) Quercetin-3-O-robinoside [R=*O*-robinoside]
8) Quercetin-3-O-rutinoside (Rutin) [R=*O*-rutinoside]
23) Quercetin-3-O-glucoside [R=*O*-glc]
29) Quercetin [R=H]

Flavones

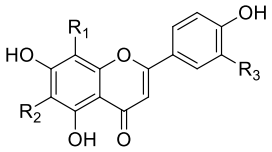

10) Chrysoeriol [R_1=R_2=H, R_3=OCH_3]
17) Vicenin-2 [R_1=R_3=*C*-glc, R_4=H]
18) Orientin [R_1=*C*-glc, R_2=H, R_3=OH]
19) Isoorientin [R_1=H, R_2=*C*-glc, R_3=OH]
21) Isovitexin [R_1=R_3=H, R_2=*C*-glc]
22) Vitexin [R_1=*C*-glc, R_2=R_3=H]
26) Luteolin [R_1=R_2=H, R_3=OH]

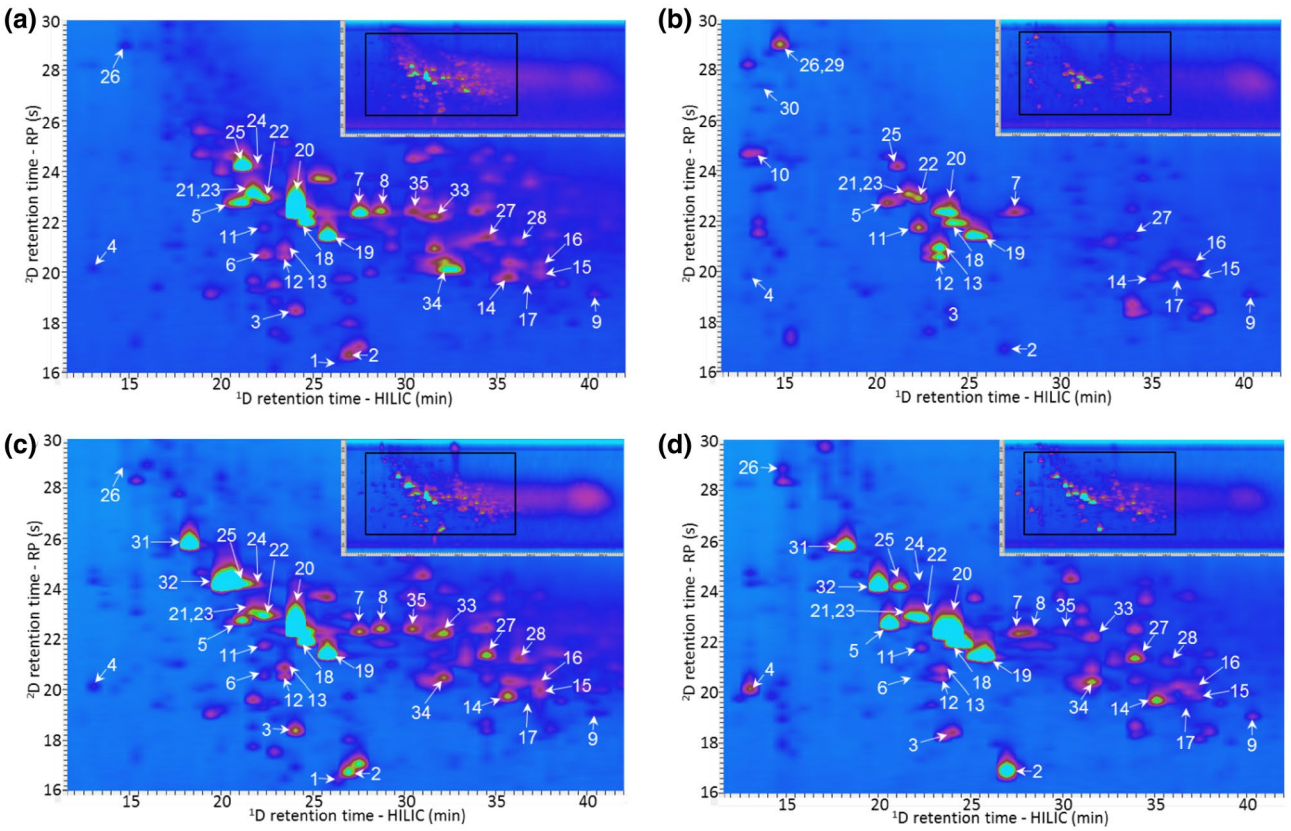

Fig. 4 Contour plots obtained at 280 nm for the HILIC × RP-LC separation of the phenolic compounds in four rooibos tea samples: unfermented (**a**) and fermented (**b**) commercial samples, and two unfermented tea samples from the Wupperthal district (**c, d**). The inserts in the top right corner show the complete contour plots with the marked sections being enlarged. Peak numbers correspond to Table 3 and Fig. 3. Figure 4d reprinted (adapted) with permission from [27]. Copyright 2018 American Chemical Society

Table 3 Characteristics of the phenolic compounds tentatively identified in the rooibos tea samples by HILIC × RP-LC−DAD-HR-MS

No.	Compound	HILIC ^{1}D t_R[a] (min)	RP-LC ^{2}D t_R[a] (s)	Molecular formula $[M-H]^-$	Exp $[M-H]^-$	Error (ppm)	MS^E fragments[b]	λ_{max} (nm)
1	Unknown: 355	26.10	16.3	$C_{15}H_{15}O_{10}$	355.0691	3.7	**192**, 135	324
2	Unknown: 357	26.68	16.9	$C_{15}H_{17}O_{10}$	357.0822	3.4	195, **151**, 135, 123	296, 318
3	1-Caffeoylglucose	23.78	18.4	$C_{15}H_{17}O_9$	341.0881	2.3	179, **135**	300
4	Catechin	16.24	19.4	$C_{15}H_{13}O_6$	289.0724	4.2	**245**	240, 276
5	Coumaric acid-*O*-glucoside	20.88	22.8	$C_{15}H_{17}O_8$	325.0917	−1.8	163, **119**	278
6	Phenylpropenoic acid glucoside (PPAG)	22.04	20.6	$C_{15}H_{17}O_8$	325.0926	0.9	161, **119**	262
7	Quercetin-3-*O*-robinobioside	27.26	22.3	$C_{27}H_{29}O_{16}$	609.1484	−1.1	**563**, 415, 301	256, 354
8	Quercetin-3-*O*-rutinoside (rutin)	28.42	22.4	$C_{27}H_{29}O_{16}$	609.1487	5.1	**563**, 460, 323, 301	256, 354
9	Luteolin-6,8-di-*C*-hexoside	40.02	19.1	$C_{27}H_{29}O_{16}$	609.1428	−4.6	**339**	348
10	Chrysoeriol	13.34	24.7	$C_{16}H_{11}O_6$	299.0541	−5.0	**284**, 125	246, 322
11	(R)-eriodictyol-8-*C*-glucopyranoside	22.04	21.7	$C_{21}H_{21}O_{11}$	449.1076	−1.8	431, **329**, 193	244, 286
12	(S)-eriodictyol-6-*C*-glucopyranoside	23.20	20.6	$C_{21}H_{21}O_{11}$	449.1064	−4.5	441, **329**, 192	238, 290
13	(R)-eriodictyol-6-*C*-glucopyranoside	23.20	20.9	$C_{21}H_{21}O_{11}$	449.1074	−2.2	373, **329**, 265, 197	238, 288
14	Luteolin-*C*-glucoside-*C*-arabinoside	35.38	19.8	$C_{26}H_{27}O_{15}$	579.1316	−5.9	**369**	268, 340
15	Luteolin-*C*-glucoside-*C*-arabinoside	37.12	19.9	$C_{26}H_{27}O_{15}$	579.1376	4.5	**369**	246, 270, 344
16	Luteolin-*C*-glucoside-*C*-arabinoside	37.12	20.3	$C_{26}H_{27}O_{15}$	579.1385	6.0	**369**	246,270, 346
17	Apigenin-6,8-di-*C*-glycoside (vicenin-2)	36.54	19.4	$C_{27}H_{29}O_{15}$	593.1520	2.4	**353**	242, 274, 324
18	Orientin	24.36	22.0	$C_{21}H_{19}O_{11}$	447.0936	2.0	357, 331, **327**	256, 266, 348
19	Isoorientin	25.52	21.4	$C_{21}H_{19}O_{11}$	447.0935	1.8	**357**, 327	228, 268, 348
20	Aspalathin	23.78	22.4	$C_{21}H_{23}O_{11}$	451.1247	1.6	361, **331**, 289, 209	288
21	Isovitexin	21.46	23.1	$C_{21}H_{19}O_{10}$	431.0974	−1.9	**311**, 281, 209	258, 350
22	Vitexin	22.04	22.9	$C_{21}H_{19}O_{10}$	431.0997	4.4	341, **311**, 149	270, 336
23	Quercetin-3-*O*-glucoside (isoquercitrin)	21.46	23.1	$C_{21}H_{19}O_{12}$	463.0877	3.7	315, **301**, 164, 151	258, 350
24	Nothofagin	20.88	24.4	$C_{21}H_{23}O_{10}$	435.1314	5.3	345, **315**, 185	232, 286
25	Phenylpropenoic acid glucoside derivative	20.30	24.6	$C_{21}H_{25}O_{12}$	469.1366	4.3	367, 325, 163, **119**	276
26	Luteolin	14.50	29.0	$C_{15}H_9O_6$	285.0409	3.5	225, **179**, 159	252, 344
27	Di-*C*-hexosyl derivative of aspalathin	34.22	21.4	$C_{27}H_{33}O_{16}$	613.1744	−4.1	**493**, 434, 403, 373	238, 286
28	Di-*C*-hexosyl derivative of aspalathin	35.96	21.2	$C_{27}H_{33}O_{16}$	613.1786	2.8	**493**	240, 280
29	Quercetin	14.50	29.0	$C_{15}H_9O_7$	301.0344	−1.3	179, **151**	254, 266
30	Secoisolariciresinol	13.92	27.3	$C_{20}H_{25}O_6$	361.1626	−6.9	**343**, 164	250, 280
31	Phloridzin	17.98	25.8	$C_{21}H_{23}O_{10}$	435.1310	4.4	**273**, 167, 125	226, 284
32	Sieboldin positional isomer	19.72	24.5	$C_{21}H_{23}O_{11}$	451.1247	1.9	**289**, 167	226, 286
33	Aspalathin dimer	31.90	22.2	$C_{42}H_{45}O_{22}$	901.2408	0.7	**881**, 781, 493	234, 284
34	Aspalathin derivative	31.90	20.5	$C_{26}H_{29}O_{15}$	581.1514	1.4	**491**, 371, 331, 289	236, 284
35	Unknown: 1027	30.16	22.4	$C_{51}H_{47}O_{23}$	1027.2546	3.7	**749**, 723, 396, 184	234, 284

Peak numbers correspond to Figs. 3 and 4

[a] t_R: retention time

[b] MS^E base peak ions in bold

peak areas for orientin (**18**) and isoorientin (**19**) between the fermented and unfermented samples were roughly similar, the levels of aspalathin (**20**) and the aspalathin dimer (**34**) in the fermented sample were significantly lower, while those of the three flavanones (**11, 12** and **13**) were higher. The lower concentration of rutin (**8**) in the fermented sample, as well as the detection of the quercetin aglycone (**29**), may be explained by the partial hydrolysis of rutin during fermentation [45]. Compared to the commercial tea sample, the unfermented samples of two ecotypes from Wupperthal are clearly differentiated based on their high contents of phloridzin (**31**) and the Sieboldin positional isomer (**32**). These two compounds are unique to tea species from the Wupperthal district [25].

Wine and Grape Samples

Phenolic compounds are important constituents of wine since they contribute to organoleptic properties such as astringency, bitterness, colour and ageing potential [46], and are also associated with the health benefits related to moderate wine consumption [47, 48]. The phenolic composition of wines is largely determined by that of the grapes used for production, as well as by winemaking practices. Phenolic profiles of grapes differ between cultivars, but are also influenced by environmental factors such as geographical location and microclimatic conditions [49].

In this study, Shiraz grapes of the 2016 harvest and red wine produced from these grapes were analysed to confirm the applicability of the proposed methodology for both types of samples. An ether extraction was performed to concentrate the compounds of interest and to remove the unwanted anthocyanins and higher molecular weight polyphenols. Since this extraction also removed compounds highly retained in the HILIC dimension, the ^{1}D HILIC analysis time for these samples was shortened from 70 to 50 min (Table 1).

The UV contour plots (280 nm and 360 nm) obtained for the HILIC × RP-LC−MS analysis of the grape and wine samples are presented in Fig. 6. In total 49 compounds were assigned, of which 45 (21 flavonols, 8 flavanonols, 8 phenolic acids, 3 stilbenes and 5 procyanidins) were tentatively identified based on the UV spectra, retention times, high resolution MS data and MS^{E} fragmentation patterns (Table 4).

The contour plots presented in Fig. 6 also allow for the evaluation of differences in phenolic contents between grapes and wine. As expected, the phenolic profile of the wine differed significantly from that of the grapes used for its production (Fig. 6a, b) [50]. Flavonols, one class of grape flavonoids which mainly occur in the berry skins [46], is of particular interest in this regard [50]. For visual comparison of the flavonol profiles of the samples, contour plots at 360 nm are presented in Fig. 6c, d, since this wavelength is selective for flavonols (and anthocyanins, not present in the ether extracts analysed here). From these figures, the previously reported [51] group-type separation of flavonols by HILIC × RP-LC is also evident. The wine sample contained noticeably higher levels of the flavonol aglycones (**1–6**), flavanonol aglycones (**19–25**) and free phenolic acids (**26–33**, Fig. 6a, c). On the other hand, the grapes contained much higher levels of flavonol-glycosides (**7–18**) and di-glycosylated flavonol species (**43–47**), which were not detected in the wine (Fig. 6b, d). This can be explained by the acid-catalysed hydrolysis of the flavonol-glycoside bond during wine production, which leads to higher concentrations of the aglycones in the wine compared to the grapes [50].

Performance of the Kinetically Optimised HILIC × RP-LC-MS Methodology

To assess the performance of the HILIC × RP-LC separations, the practical peak capacities and orthogonality were calculated for each sample. Details on how these calculations were performed can be found in Sect. S2 in the SI, and a summary of the values obtained is presented in Table S3.

Experimentally determined ^{1}D peak capacities corrected for undersampling ($^{1}n'_{c}$) were significantly higher, especially for the grape seed and rooibos tea samples, than the predicted value of 43 (Fig. S2, SI). This underestimation of ^{1}D performance was expected, since plate height data measured on a diol column were used in the kinetic prediction, while a more efficient amide column was used in the experiments. Slightly larger average ^{1}D peak widths were measured for the grape and wine samples, likely due to the shallow gradient employed in these analyses; much lower $^{1}n'_{c}$ are also due to the shorter ^{1}D gradients used for these samples. In the ^{2}D, experimentally determined peak capacities for the superficially porous 1.7 µm and fully porous 1.8 µm columns were only 11% and 14% lower, respectively, than the values predicted using plate height data for procyanidins (Fig. S2, SI). The relatively good agreement between predictions and measured performance for the rooibos tea, wine and grape samples confirms the suitability of oligomeric procyanidins as reference compounds to derive optimal experimental conditions for a much wider range of phenolics. Practical 2D peak capacities corrected for undersampling ($n'_{c,2D}$) ranged from 2200 for 50 min analyses to 4400 for 70 min analyses (Table S3). These values do not provide a complete estimate of separation performance, however, since orthogonality is not accounted for. Therefore, the orthogonality of the separations reported in this work was estimated using both the asterisk [52] and convex hull methods [53]. Orthogonality values determined in this manner ranged between 61 and 69% for the asterisk method, while surface coverage values obtained by the convex hull method

Table 4 Characteristics of the phenolic compounds tentatively identified in the wine and grape samples by HILIC × RP-LC−DAD-HR-MS

No.	Compound	HILIC $^{1}D\ t_R$[a] (min)	RP-LC $^{2}D\ t_R$[a] (s)	Molecular formula $[M-H]^-$	Exp. $[M-H]^-$	Error (ppm)	MS^E fragments[b]	λ_{max} (nm)
1	Kaempferol	12.76	31.6	$C_{15}H_9O_6$	285.0399	4.9	**228**, 213, 172, 151	264, 366
2	Isorhamnetin	12.76	26.0	$C_{16}H_{11}O_7$	315.0520	4.8	**265**, 271, 217, 151	254, 370
3	Syringetin	12.76	25.2	$C_{17}H_{13}O_8$	345.0625	4.3	315, **153**, 96	254, 370
4	Laricitrin	16.82	29.0	$C_{16}H_{11}O_8$	331.0456	0.6	**316**, 151, 179	254, 370
5	Quercetin	16.82	29.0	$C_{15}H_9O_7$	301.0348	5.3	179, **151**	256, 370
6	Myricetin	20.88	26.0	$C_{15}H_9O_8$	317.0300	0.9	301, **179**, 151, 137	254, 372
7	Quercetin-3-*O*-galactoside/ glucoside	30.74	23.0	$C_{21}H_{19}O_{12}$	463.0877	3.4	**300**, 271, 180, 163	258, 356
8	Laricitrin-3-*O*-glucoside	31.35	24.1	$C_{22}H_{21}O_{13}$	493.0995	2.6	**330**, 331, 301, 171	280, 384
9	Laricitrin-3-*O*-galactoside	31.32	23.2	$C_{22}H_{21}O_{13}$	493.0997	3.0	**331**, 330, 301, 285	256, 358
10	Kaempferol-3-*O*-galactoside	26.71	24.7	$C_{21}H_{19}O_{11}$	447.0897	6.3	**285**	256, 296, 350
11	Kaempferol-3-*O*-glucoside	27.87	25.2	$C_{21}H_{19}O_{11}$	447.0919	−1.8	**227**, 125	356
12	Isorhamnetin-3-*O*-galactoside/ glucoside	27.26	25.5	$C_{22}H_{21}O_{12}$	477.1033	4.0	**447**, 314, 315, 270	256, 318, 356
13	Quercetin-3-*O*-glucuronide	32.48	23.1	$C_{21}H_{17}O_{13}$	477.0676	1.5	**301**, 175, 113	256, 356
14	Syringetin-3-*O*-galactoside/ glucoside	27.26	25.5	$C_{23}H_{23}O_{13}$	507.1146	1.4	**345**, 261, 201	256, 318, 356
15	Myricetin-3-*O*-galactoside	34.80	21.6	$C_{21}H_{19}O_{13}$	479.0821	−1.0	**316**, 301	258, 356
16	Myricetin-3-*O*-glucoside	35.38	21.9	$C_{21}H_{19}O_{13}$	479.0824	−0.4	**316**, 151	258, 356
17	Quercetin-3-*O*-(6″-acetyl)-glucoside	24.94	27.0	$C_{23}H_{21}O_{13}$	505.0984	0.4	**330**, 128	312
18	Syringetin-3-*O*-(6″-acetyl)-glucoside	22.62	28.0	$C_{25}H_{25}O_{14}$	549.1232	−2.2	**515**, 445, 299	258, 310, 358
19	Dihydro-quercetin	17.40	24.5	$C_{15}H_{11}O_7$	303.0509	1.3	**285**, 153, 125	288
20	Dihydro-laricitrin	21.48	23.2	$C_{16}H_{13}O_8$	333.0613	0.9	**193**, 125	290
21	Unknown: 319	22.04	21.7	$C_{15}H_{11}O_8$	319.0456	0.6	301, **193**, 179, 125	290
22	Dihydro-myricetin	24.90	20.5	$C_{15}H_{11}O_8$	319.0457	0.9	**317**, 193, 165, 125	278
23	Dihydro-isorhamnetin	17.40	25.3	$C_{16}H_{13}O_7$	317.0669	2.5	**315**, 165, 123	272, 320
24	Dihydro-syringetin	17.40	25.6	$C_{17}H_{15}O_8$	347.0783	4.6	327, 261, **165**, 153	370, 320
25	Dihydro-kaempferol	15.08	27.3	$C_{15}H_{11}O_6$	287.0558	0.7	**227**, 191	304
26	Gallic acid	23.20	14.9	$C_7H_5O_5$	169.0122	−8.9		270
27	Vanillic acid	12.18	27.3	$C_8H_7O_4$	167.0346	1.2	147, 119	259
28	Syringic acid	13.92	24.0	$C_9H_9O_5$	197.0453	1.5	169, **124**	272
29	Caffeic acid	16.82	20.8	$C_9H_7O_4$	179.0353	5.0	**135**	324
30	Fertaric acid	22.04	20.8	$C_{14}H_{13}O_9$	325.0531	−0.9	**193**	278
31	Coutaric acid	23.20	19.4	$C_{13}H_{11}O_8$	295.0465	3.7	273, **163**	314
32	Caftaric acid	27.26	17.6	$C_{13}H_{11}O_9$	311.0413	3.2	179, **150**, 149	328
33	*p*-Coumaric acid	12.76	23.5	$C_9H_7O_3$	163.0397	1.2	**119**	300
34	Resveratrol	12.76	29.9	$C_{14}H_{11}O_3$	227.0718	4.4	201, 185, **159**, 143	280
35	*trans*-piceid	27.84	24.3	$C_{20}H_{21}O_8$	389.1214	−5.7	**227**	312
36	*cis*-piceid	27.84	25.5	$C_{20}H_{21}O_8$	389.1223	−3.3	315, **227**	316
37	Catechin	21.46	19.3	$C_{15}H_{13}O_6$	289.0726	4.8	**273**, 245, 203, 193	278
38	Epicatechin	21.46	20.8	$C_{15}H_{13}O_6$	289.0715	1.0	**273**, 245, 203, 193	278
39	Procyanidin dimer	30.16	21.2	$C_{30}H_{25}O_{12}$	577.1360	2.4	**289**	276
40	Procyanidin dimer	33.64	19.7	$C_{30}H_{25}O_{12}$	577.1346	1.4	**289**	276
41	Procyanidin dimer	34.22	18.0	$C_{30}H_{25}O_{12}$	577.1371	4.3	**289**	278
42	Unknown: 363	19.72	31.6	$C_{15}H_{17}O_8$	363.0709	−1.9	345, 197, 183, **165**	280
43	Laricitrin-3-*O*-rhamnosyl-hexoside	25.52	26.0	$C_{17}H_{15}O_9$	639.1379	4.5	599, **331**, 305, 301	248, 314

Table 4 (continued)

No.	Compound	HILIC ^{1}D t_R[a] (min)	RP-LC ^{2}D t_R[a] (s)	Molecular formula $[M-H]^-$	Exp. $[M-H]^-$	Error (ppm)	MS^E fragments[b]	λ_{max} (nm)
44	Isorhamnetin-3-*O*-rhamnosyl-hexoside	22.62	25.2	$C_{31}H_{27}O_{15}$	623.1380	−3.4	357, **315**, 266	240, 314
45	Syringetin-3-*O*-rhamnosyl-hexoside	22.62	29.0	$C_{31}H_{27}O_{14}$	653.1520	2.1	387, **345**, 365, 153	240, 314
46	Dihydro-isorhamnetin-3-*O*-dihexose	26.10	29.0	$C_{32}H_{29}O_{15}$	641.1550	6.9	**315**	230, 298
47	Dihydro-syringetin-3-*O*-dihexose	26.10	26.0	$C_{31}H_{29}O_{15}$	671.1624	1.8	**345**	230, 298
48	Unknown: 685	24.35	23.0	$C_{32}H_{31}O_{16}$	685.1780	1.6	359, **345**	244, 312
49	Unknown: 685	26.68	24.1	$C_{33}H_{33}O_{16}$	685.1785	2.3	359, **345**, 325	242, 312

[a] t_R: retention time

[b] MS^E base peak ions in bold

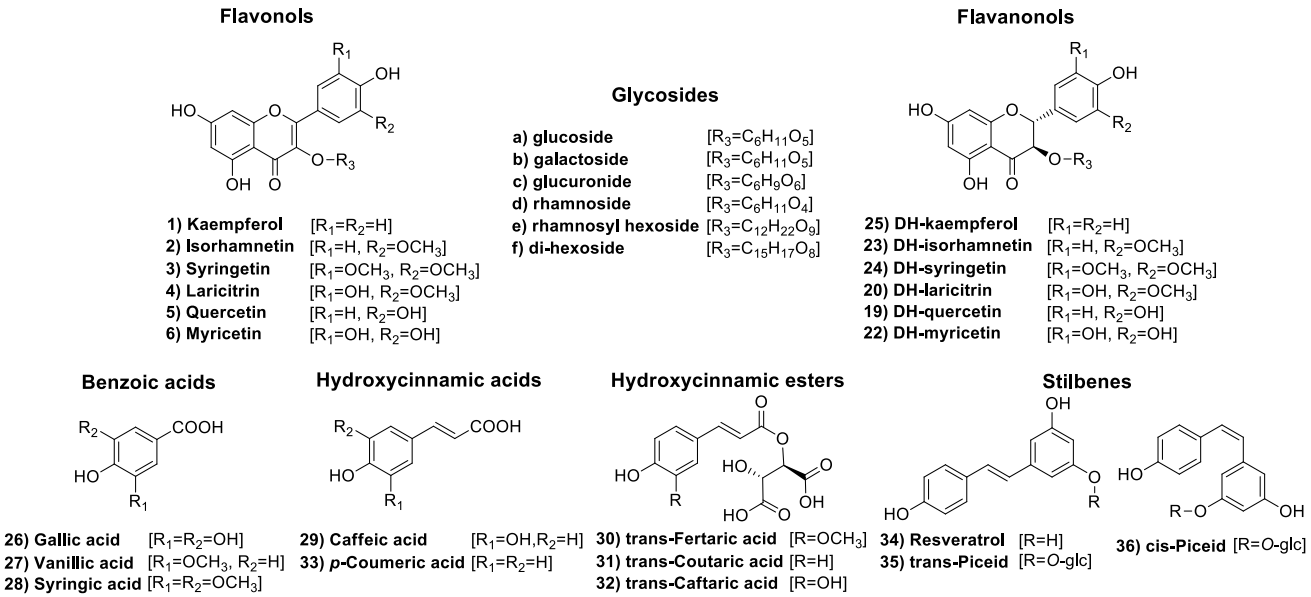

Fig. 5 Structures of the phenolic compounds tentatively identified in the wine and grape samples. Numbers correspond to Fig. 6 and Table 4. *O-glc O*-linked glucoside, *DH* dihydro

were between 50 and 71% (Table S3), confirming the suitability of HILIC × RP-LC systems for phenolic analysis. Combining $n'_{c,2D}$ and surface coverage values, the average practical peak capacity corrected for undersampling and finite surface coverage [53] is 1900 for the methodology reported here, which represents excellent performance for analysis times in the order of an hour. Note though that a generic ^{2}D gradient was used in the present work to minimise method development time. Further fine-tuning of the ^{2}D gradient according to the composition of each sample, including the possibility of using shifting gradients [15, 43], is recommended to improve kinetically optimised configurations for given applications.

Conclusions

In this study, a predictive optimisation protocol incorporating fixed modulation requirements to limit injection band broadening was used to derive kinetically optimised experimental conditions for the online HILIC × RP-LC-DAD-MS analysis of phenolic compounds. To demonstrate the general applicability of the proposed methodology, several natural products (grape seeds, rooibos tea, grapes and wine) containing diverse phenolic constituents were analysed. The results confirm that excellent separation of condensed tannins, flavonols, flavones, flavanones,

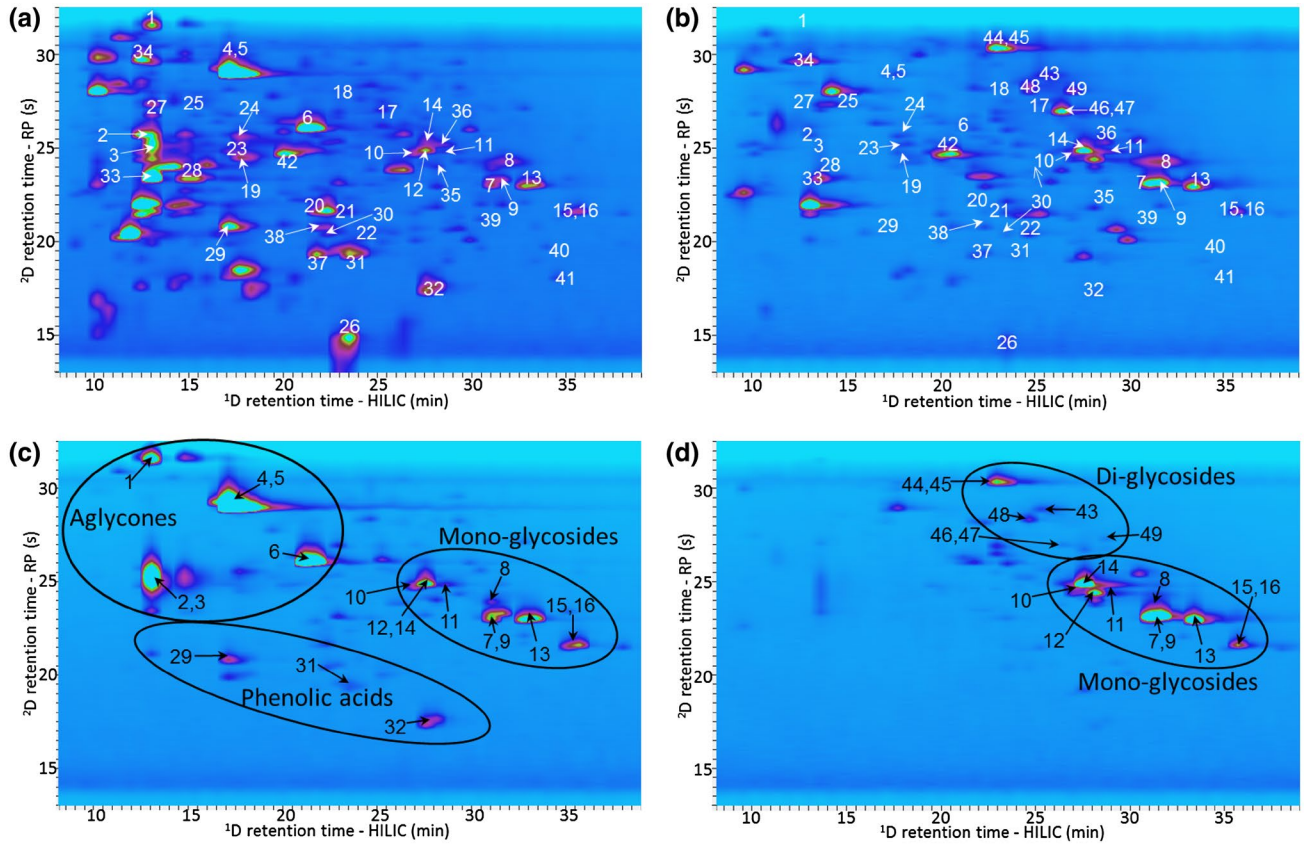

Fig. 6 Contour plots obtained at 280 nm for the HILIC × RP-LC separation of the phenolics in ether extracts of **a** a Shiraz red wine sample, and **b** the grapes from which the wine was produced. The corresponding contour plots at 360 nm are shown in (**c**) and (**d**). Peak numbers correspond to Table 4 and Fig. 5

flavanonols, (dihydro)chalcones, stilbenes and phenolic acids can be obtained using the proposed methodology, as confirmed by practical peak capacities in the order of 2000 for 50–70 min analysis times.

Hyphenation of optimised HILIC × RP-LC separation to diode array and HR-MS detection enabled the detection of 156 phenolic compounds (72 in grape seeds, 35 in rooibos tea and 49 in wine and grapes), of which 149 were tentatively identified based on UV spectra, HILIC and RP-LC retention times, high resolution MS data and MS^E fragmentation patterns. The presence of a relatively large number of unidentified minor constituents in each of the investigated samples highlights the complexity of natural phenolic mixtures, and the importance of developing more powerful analytical tools to investigate these. UV contour plots, furthermore, allow visual comparison of the phenolic profiles, thereby facilitating identification of differences between samples.

In summary, the kinetically optimised HILIC × RP-LC–DAD-HR-MS methodology based on dilution of the ^{1}D effluent and large volume injection offers a powerful and relatively fast methodology for the detailed screening of phenolic content in a range of natural products. While further fine-tuning of the methodology for particular samples might be required for detailed investigation of these, the reported protocol represents a suitable generic starting point for such studies also.

Acknowledgements The authors would like to acknowledge financial support from Sasol (Collaborative Grant to AdV) and the National Research Foundation of South Africa (Grants 98897 to AdV, 91436 to AGJT and post-graduate bursary to MM). The authors gratefully acknowledge Agilent Technologies (University Relations & External Research) for the donation of some of the instrumentation used in this work (Research Gift #3888 to AdV). Maria A. Stander is thanked for providing the rooibos samples, and Wessel J. Du Toit for the grape and wine samples.

Funding This study was funded by Sasol (Collaborative Grant to AdV), the National Research Foundation of South Africa (Grants 98897 to AdV, 91436 to AGJT and bursary to MM), Agilent Technologies (Research Gift #3888 to AdV).

Compliance with ethical standards

Conflict of interest The authors declare that they have no conflict of interest.

Ethical approval This article does not contain any studies with human participants or animals performed by any of the authors.

References

1. Bravo L (1998) Polyphenols: chemistry, dietary sources, metabolism, and nutritional significance. Nutr Rev 56:1–22
2. Kalili KM, de Villiers A (2011) Recent developments in the HPLC separation of phenolic compounds. J Sep Sci 34:854–876. https://doi.org/10.1002/jssc.201000811
3. Tranchida PQ, Donato P, Cacciola F et al (2013) Potential of comprehensive chromatography in food analysis. Trends Anal Chem 52:186–205. https://doi.org/10.1016/j.trac.2013.07.008
4. de Villiers A, Venter P, Pasch H (2015) Recent advances and trends in the liquid-chromatography-mass spectrometry analysis of flavonoids. J Chromatogr A 1430:16–78. https://doi.org/10.1016/j.chroma.2015.11.077
5. Schoenmakers PJ, Vivó-Truyols G, Decrop WMC (2006) A protocol for designing comprehensive two-dimensional liquid chromatography separation systems. J Chromatogr A 1120:282–290. https://doi.org/10.1016/j.chroma.2005.11.039
6. Fairchild JN, Horváth K, Guiochon G (2009) Approaches to comprehensive multidimensional liquid chromatography systems. J Chromatogr A 1216:1363–1371. https://doi.org/10.1016/j.chroma.2008.12.073
7. Gu H, Huang Y, Carr PW (2011) Peak capacity optimization in comprehensive two dimensional liquid chromatography: a practical approach. J Chromatogr A 1218:64–73. https://doi.org/10.1016/j.chroma.2010.10.096
8. Vivó-Truyols G, Van Der Wal S, Schoenmakers PJ (2010) Comprehensive study on the optimization of online two-dimensional liquid chromatographic systems considering losses in theoretical peak capacity in first- and second-dimensions: a pareto-optimality approach. Anal Chem 82:8525–8536. https://doi.org/10.1021/ac101420f
9. Kalili KM, de Villiers A (2013) Systematic optimisation and evaluation of online, off-line and stop-flow comprehensive hydrophilic interaction chromatography × reversed phase liquid chromatographic analysis of procyanidins, part I: theoretical considerations. J Chromatogr A 1289:58–68. https://doi.org/10.1016/j.chroma.2013.03.008
10. Sarrut M, D'Attoma A, Heinisch S (2015) Optimization of conditions in online comprehensive two-dimensional reversed phase liquid chromatography: experimental comparison with one-dimensional reversed phase liquid chromatography for the separation of peptides. J Chromatogr A 1421:48–59. https://doi.org/10.1016/j.chroma.2015.08.052
11. Sarrut M, Rouvière F, Heinisch S (2017) Theoretical and experimental comparison of one dimensional versus online comprehensive two dimensional liquid chromatography for optimized subhour separations of complex peptide samples. J Chromatogr A 1498:183–195. https://doi.org/10.1016/j.chroma.2017.01.054
12. Pirok BWJ, Pous-Torres S, Ortiz-Bolsico C et al (2016) Program for the interpretive optimization of two-dimensional resolution. J Chromatogr A 1450:29–37. https://doi.org/10.1016/j.chroma.2016.04.061
13. de Villiers A, Kalili KM (2016) Comprehensive two-dimensional hydrophilic interaction chromatography × reversed phase liquid chromatography (HILIC × RP–LC). In: Grushka E, Grinberg N (eds) Advances in chromatography, 53rd edn. CRC Press, Boca Raton, pp 217–299
14. Cacciola F, Farnetti S, Dugo P et al (2017) Comprehensive two-dimensional liquid chromatography for polyphenol analysis in foodstuffs. J Sep Sci 40:7–24. https://doi.org/10.1002/jssc.201600704.This
15. Muller M, Tredoux AGJ, de Villiers A (2018) Predictive kinetic optimisation of HILIC × RP-LC separations: experimental verification and application to phenolic analysis. J Chromatogr A 1571:107–120. https://doi.org/10.1016/j.chroma.2018.08.004
16. Stoll DR, Sajulga RW, Voigt BN et al (2017) Simulation of elution profiles in liquid chromatography—II: investigation of injection volume overload under gradient elution conditions applied to second dimension separations in two-dimensional liquid chromatography. J Chromatogr A. https://doi.org/10.1016/j.chroma.2017.07.041
17. Filgueira MR, Huang Y, Witt K et al (2011) Improving peak capacity in fast online comprehensive two-dimensional liquid chromatography with post first dimension flow-splitting. Anal Chem 83:9531–9539
18. Stoll DR, Talus ES, Harmes DC, Zhang K (2015) Evaluation of detection sensitivity in comprehensive two-dimensional liquid chromatography separations of an active pharmaceutical ingredient and its degradants. Anal Bioanal Chem 407:265–277. https://doi.org/10.1007/s00216-014-8036-9
19. Li Q, Lynen F, Wang J et al (2012) Comprehensive hydrophilic interaction and ion-pair reversed-phase liquid chromatography for analysis of di- to deca-oligonucleotides. J Chromatogr A 1255:237–243. https://doi.org/10.1016/j.chroma.2011.11.062
20. De Vos J, Eeltink S, Desmet G (2015) Peak refocusing using subsequent retentive trapping and strong eluent remobilization in liquid chromatography: a theoretical optimization study. J Chromatogr A 1381:74–86. https://doi.org/10.1016/j.chroma.2014.12.082
21. Van de Ven HC, Gargano AFG, Van der Wal SJ, Schoenmakers PJ (2016) Switching solvent and enhancing analyte concentrations in small effluent fractions using in-column focusing. J Chromatogr A 1427:90–95. https://doi.org/10.1016/j.chroma.2015.11.082
22. Fornells E, Barnett B, Bailey M et al (2018) Evaporative membrane modulation for comprehensive two-dimensional liquid chromatography. Anal Chim Acta 1000:303–309. https://doi.org/10.1016/j.aca.2017.11.053
23. Tian H, Xu J, Xu Y, Guan Y (2006) Multidimensional liquid chromatography system with an innovative solvent evaporation interface. J Chromatogr A 1137:42–48. https://doi.org/10.1016/j.chroma.2006.10.005
24. Kennedy JA, Jones GP (2001) Analysis of proanthocyanidin cleavage products following acid-catalysis in the presence of excess phloroglucinol. J Agric Food Chem 49:1740–1746. https://doi.org/10.1021/jf001030o
25. Stander MA, Van Wyk B-E, Taylor MJC, Long HS (2017) Analysis of phenolic compounds in rooibos tea (*Aspalathus linearis*) with a comparison of flavonoid-based compounds in natural populations of plants from different regions. J Agric Food Chem 65:10270–10281. https://doi.org/10.1021/acs.jafc.7b03942
26. Moss R, Mao Q, Taylor D, Saucier C (2013) Investigation of monomeric and oligomeric wine stilbenoids in red wines by ultra-high-performance liquid chromatography/electrospray ionization quadrupole time-of-flight mass spectrometry. Rapid Commun Mass Spectrom 27:1815–1827. https://doi.org/10.1002/rcm.6636
27. Venter P, Muller M, Vestner J et al (2018) Comprehensive three-dimensional LC × LC × ion mobility spectrometry separation combined with high-resolution MS for the analysis of complex samples. Anal Chem 90:11643–11650. https://doi.org/10.1021/acs.analchem.8b03234
28. Kalili KM, Cabooter D, Desmet G, de Villiers A (2012) Kinetic optimisation of the reversed phase liquid chromatographic separation of proanthocyanidins on sub-2 µm and superficially porous phases. J Chromatogr A 1236:63–76. https://doi.org/10.1016/j.chroma.2012.02.067

29. Willemse CM, Stander MA, Vestner J et al (2015) Comprehensive two-dimensional hydrophilic interaction chromatography (HILIC) × reversed-phase liquid chromatography coupled to high-resolution mass spectrometry (RP-LC-UV-MS) analysis of anthocyanins and derived pigments in red wine. Anal Chem 87:12006–12015. https://doi.org/10.1021/acs.analchem.5b03615
30. Terblanche E (2017) Development of novel methods for tannin quantification in grapes and wine. University of Stellenbosch
31. Prieur C, Rigaud J, Cheynier V, Moutounet M (1994) Oligomeric and polymeric from grape seeds. Phytochemistry 36:781–784
32. Kalili KM, Vestner J, Stander M, De Villiers A (2013) Toward unraveling grape tannin composition: application of online hydrophilic interaction chromatography × reversed-phase liquid chromatography-time-of-flight mass spectrometry for grape seed analysis. Anal Chem 85:9107–9115. https://doi.org/10.1021/ac401896r
33. de Freitas VAP, Glories Y, Laguerre M (1998) Incidence of molecular structure in oxidation of grape seed procyanidins. J Agric Food Chem. https://doi.org/10.1021/jf970468u
34. Montero L, Herrero M, Prodanov M et al (2013) Characterization of grape seed procyanidins by comprehensive two-dimensional hydrophilic interaction × reversed phase liquid chromatography coupled to diode array detection and tandem mass spectrometry. Anal Bioanal Chem 405:4627–4638. https://doi.org/10.1007/s00216-012-6567-5
35. Kalili KM, De Smet S, Van Hoeylandt T et al (2014) Comprehensive two-dimensional liquid chromatography coupled to the ABTS radical scavenging assay: a powerful method for the analysis of phenolic antioxidants. Anal Bioanal Chem 406:4233–4242. https://doi.org/10.1007/s00216-014-7847-z
36. Joubert E, Gelderblom WCA, Louw A, de Beer D (2008) South African herbal teas: *Aspalathus linearis, Cyclopia* spp. and *Athrixia phylicoides*—a review. J Ethnopharmacol 119:376–412. https://doi.org/10.1016/j.jep.2008.06.014
37. Joubert E, Schultz H (2006) Production and quality aspects of rooibos tea and related products. A review. J Appl Bot Food Qual 80:138–144
38. Beelders T, Kalili KM, Joubert E et al (2012) Comprehensive two-dimensional liquid chromatographic analysis of rooibos (*Aspalathus linearis*) phenolics. J Sep Sci 35:1808–1820. https://doi.org/10.1002/jssc.201200060
39. Beelders T, Sigge GO, Joubert E et al (2012) Kinetic optimisation of the reversed phase liquid chromatographic separation of rooibos tea (*Aspalathus linearis*) phenolics on conventional high performance liquid chromatographic instrumentation. J Chromatogr A 1219:128–139. https://doi.org/10.1016/j.chroma.2011.11.012
40. Walters NA, de Villiers A, Joubert E, de Beer D (2017) Improved HPLC method for rooibos phenolics targeting changes due to fermentation. J Food Compos Anal 55:20–29. https://doi.org/10.1016/j.jfca.2016.11.003
41. Walters NA, de Villiers A, Joubert E, de Beer D (2017) Phenolic profiling of rooibos using off-line comprehensive normal phase countercurrent chromatography × reversed phase liquid chromatography. J Chromatogr A 1490:102–114. https://doi.org/10.1016/j.chroma.2017.02.021
42. Arries WJ, Tredoux AGJ, de Beer D et al (2017) Evaluation of capillary electrophoresis for the analysis of rooibos and honeybush tea phenolics. Electrophoresis 38:897–905. https://doi.org/10.1002/elps.201600349
43. Bedani F, Kok WT, Janssen HG (2009) Optimal gradient operation in comprehensive liquid chromatography × liquid chromatography systems with limited orthogonality. Anal Chim Acta 654:77–84. https://doi.org/10.1016/j.aca.2009.06.042
44. Krafczyk N, Glomb MA (2008) Characterization of phenolic compounds in rooibos tea. J Agric Food Chem 56:3368–3376. https://doi.org/10.4067/S0718-221X2015005000043
45. Bramati L, Aquilano F, Pietta P (2003) Unfermented rooibos tea: quantitative characterization of flavonoids by HPLC-UV and determination of the total antioxidant activity. J Agric Food Chem 51:7472–7474. https://doi.org/10.1021/jf0347721
46. Monagas M, Bartolomé B, Gómez-Cordovés C (2005) Updated knowledge about the presence of phenolic compounds in wine. Crit Rev Food Sci Nutr 45:85–118. https://doi.org/10.1080/10408690490911710
47. Fernández-Pachón MS, Villaño D, García-Parrilla MC, Troncoso AM (2004) Antioxidant activity of wines and relation with their polyphenolic composition. Anal Chim Acta 513:113–118. https://doi.org/10.1016/j.aca.2004.02.028
48. Biagi M, Bertelli AAE (2015) Wine, alcohol and pills: what future for the French paradox? Life Sci 131:19–22. https://doi.org/10.1016/j.lfs.2015.02.024
49. Price SF, Breen PJ, Valladao M, Watson BT (1995) cluster sun exposure and quercetin in pinot noir grapes and wine. Am J Enol Vitic 46:187–194
50. Castillo-Muñoz N, Gómez-Alonso S, García-Romero E, Hermosín-Gutiérrez I (2007) Flavonol profiles of *Vitis vinifera* red grapes and their single-cultivar wines. J Agric Food Chem 55:992–1002. https://doi.org/10.1021/jf062800k
51. Kalili KM, de Villiers A (2010) Off-line comprehensive two-dimensional hydrophilic interaction × reversed phase liquid chromatographic analysis of green tea phenolics. J Sep Sci 33:853–863. https://doi.org/10.1002/jssc.200900673
52. Camenzuli M, Schoenmakers PJ (2014) A new measure of orthogonality for multi-dimensional chromatography. Anal Chim Acta 838:93–101. https://doi.org/10.1016/j.aca.2014.05.048
53. Semard G, Peulon-agasse V, Bruchet A et al (2010) Convex hull: a new method to determine the separation space used and to optimize operating conditions for comprehensive two-dimensional gas chromatography. J Chromatogr A 1217:5449–5454. https://doi.org/10.1016/j.chroma.2010.06.048